Materials Science & Engineering A 823 (2021) 141631

Contents lists available at ScienceDirect

Materials Science & Engineering A

journal homepage: www.elsevier.com/locate/msea

Ultrastrong medium entropy alloy with simultaneous strength-ductility improvement via heterogeneous nanocrystalline structures

Fei Yin [a,b,1], Shan Hu [c,1], Rong Xu [c], Seng Xiang [d], Lin Hua [a,b,**], Gary J. Cheng [d,*]

[a] Hubei Key Laboratory of Advanced Technology for Automotive Components, Wuhan University of Technology, Wuhan, 430070, PR China
[b] Hubei Collaborative Innovation Center for Automotive Components Technology, Wuhan University of Technology, Wuhan, 430070, PR China
[c] School of Mechanical Engineering, Purdue University, West Lafayette, IN, 47907, USA
[d] School of Industrial Engineering, Purdue University, West Lafayette, IN, 47907, USA

ARTICLE INFO

Keywords:
Medium entropy alloy
Gradient heterogeneous nanograined structure
Cyclic thermal-dynamic solid-state physical process
Grain boundary strengthening
Strain rate sensitivity

ABSTRACT

Medium Entropy Alloy (MEA) has been of great research interests in materials science. However, the strength and ductility, like most metals, cannot be obtained in MEAs simultaneously so far, without changing their chemical compositions. Here, we present a new way to fabricate gradient heterogenous nanograined structure for overcoming strength-ductility trade-off of the equiatomic Medium Entropy Alloy (MEA) at multiple length scales. Ultrasonic assisted cyclic thermal dynamic solid-state physical process was developed to fabricate ultrastrong gradient heterogenous nanograined FeCoNi MEA structures with heterogenous nanocrystalline (NC). The microstructure and mechanical behaviors of the gradient heterogenous nanograined MEA are investigated. We studied the mechanical responses of the FeCoNi MEAs with designed crystalline structures. The yield strength of the heterogenous nanograined FeCoNi MEA (1.45 GPa) was increased by 8 times compared to that of coarse-grained FeCoNi MEA, while ductility was increased from 33% to 45% after the processing. The strengthening mechanism in the NC FeCoNi MEA is found to be dominated by grain refinement and heterogenous grain structure. We also found an identical strain rate sensitivity exponent for the FeCoNi medium entropy alloy at multiple length scales, implying that dislocation mediated deformation mechanism dominates in the heterogenous FeCoNi MEA. This study provides a new way to fabricate novel gradient heterogenous nanograined structures to achieve both high strength and ductility in MEAs and provide fundamental understanding of the mechanical strengthening and deformation mechanisms of the nanograined MEAs.

1. Introduction

High entropy alloys (HEAs) are the alloys constituting five or more principle elements in equiatomic or near-equiatomic concentrations, while those constituting 2–4 elements are defined as medium-entropy alloys (MEAs) [1]. Different from the conventional "base element" paradigm, a novel paradigm involving the mixing of multiple elements in an equiatomic or near-equiatomic composition for alloy design was proposed by Yeh et al. [2]. Even though the history of study on the HEAs and MEAs is only 15 years, they are of great research interests in materials science and engineering [1,3] due to their excellent specific strength [4], exceptional cryogenic strength and fracture toughness [5], superior mechanical performance at high temperature [6], superconductivity [7,8] and excellent radiation resistance [9] et al. Note that the equiatomic Cr–Mn–Fe–Co–Ni system is the most thoroughly studied HEAs experimentally and theoretically due to their good combination of high work-hardening rate, ultimate tensile strength and ductility [10–14]. Raabe et al. developed a strong and ductile CoNiV medium entropy alloy with fcc structure. They found that the CoNiV MEA has high resistance to corrosion and hydrogen embrittlement at ambient temperature at a strain rate of $10^{-4}s^{-1}$, due to its low hydrogen diffusivity and the deformation twinning that impedes cracks propagation [15]. Li et al. developed a new kind of $Co_2CrNi_{1.5}Al_{0.25}Ti_{0.25}$ MEA which can achieve an excellent strength-ductility combination at 293 K and 77

* Corresponding author.
** Corresponding author. Hubei Key Laboratory of Advanced Technology for Automotive Components, Wuhan University of Technology, Wuhan, 430070, PR China.
E-mail addresses: hualin@whut.edu.cn (L. Hua), gjcheng@purdue.edu (G.J. Cheng).
[1] Equal contribution to this work.

https://doi.org/10.1016/j.msea.2021.141631
Received 21 March 2021; Received in revised form 14 June 2021; Accepted 18 June 2021
Available online 2 July 2021

K by the synergy of heterogeneous grain structure (HGS) and heterogeneous precipitation (HP) by the combination of cold rolling and annealing. The yield strength of the as-fabricated MEA can reach as high as 1.73 GPa with a tensile elongation of 16% at 293 K [16]. The Cr–Mn–Fe–Co–Ni HEAs/MEAs usually exhibit poor mechanical strength. For example, the yield strength of the FeCoNi with an average grain size of 28 μm is only 190 MPa at room temperature [17]. Recently, strategies are emerging to get novel HEAs with ultrahigh strength and ductility based on FeCoNi MEA due to its outstanding intrinsic ductility. For example, Fu et al. designed a novel FeCoNiAlTi HEA based on the fcc single-phase equiatomic FeCoNi MEA in which two elements, Al and Ti, are added for getting ultrastrong HEA. Their research results indicated that the as-fabricated novel HEA has a tensile yield strength of as high as 1.86 GPa and an ultimate tensile strength of 2.52 GPa at room temperature. They attributed this ultrahigh strength to the hierarchical intragranular nanoprecipitates [18]. However, getting such an ultrastrong HEA is time consuming. The entire materials processing routine involves 45 h dry ball milling, 4 h wet ball milling, and 49 h drying of the metallic powders. Then the metallic powders were processed to get the bulk HEA using the SPS-sintering. Another example was reported by Yang et al. in 2018. They introduced high density $L1_2$ intermetallic nanoparticles in the fcc FeCoNi-base alloy system by alloying with Ti and Al additions to achieve a large "fcc + $L1_2$" dual-phase region for a dense precipitation. Their research results indicated that the developed dual-phase complex alloys exhibit superior strengths of 1.5 GPa and ductility as high as 50% in tensile at room temperature [19]. Earlier in 2016, Li et al. proposed a metastability-engineering strategy to get dual-phase HEAs overcoming the strength-ductility trade-off. The addition of the Mn element changed the phase condition of the matrix materials. The designed $Fe_{50}Mn_{30}Co_{10}Cr_{10}$ HEA has the fcc + hcp dual phase structure and exhibits a yield strength of almost 400 MPa with a ductility of 60% in tensile at ambient temperature. They pointed out that these large improvements in the mechanical properties of the $Fe_{50}Mn_{30}Co_{10}Cr_{10}$ is due to the underlying plastic accommodation and strain hardening processes [20]. These methods can increase the yield strength of the HEA/MEAs by modifying the phase condition or chemical compositions of the FeCoNi MEA. However, the time consuming to get such strong HEAs/MEAs is costly and the materials process routine is complicated and requires multiple experiments to optimize the chemical compositions of the materials. Hence, an efficient and effective method to enhance the mechanical properties and overcome the strength-ductility trade-off of the FeCoNi MEA without changing their chemical compositions is urgently required.

Nanograined metal and alloys are defined as the materials with the average grain size that of less than 100 nm [21]. They exhibit extraordinary mechanical strength due to the high-density grain boundaries working as the block for the dislocation movement during the plastic deformation [22]. However, the ductility of the free standing homogenous nanograined metal and alloys is poor. And the strength-ductility trade-off is an intrinsic "Achilles' heel" of nanograined metal and alloys [23]. Recently, study of achieving ultrastrong HEAs/MEAs by decreasing its grain size has drawn attentions from the materials scientists and engineers worldwide. Michel J.R. Haché et al. reviewed the studies on the nanostructured high entropy alloys in 2020. They pointed out that methods to get nanograined HEA/MEAs include mechanical alloying (MA), high pressure torsion (HPT) and DC magnetron co-sputtering (DCMS) [24]. Nevertheless, it is still challenging to get large-scale ultrastrong ductile bulk NC HEAs/MEAs with grain size that less than 100 nm due to the unstable nanostructure arising from the increased grain boundary energy [25,26] and the intrinsic strength-ductility trade-off of the nanostructured metal and alloys [27]. Additionally, the mechanical behaviors of the NC HEAs/MEAs at nanoscale are still unclear and an efficient and effective method to get such large-scale ultrastrong ductile bulk NC HEAs/MEAs is highly desired.

Hereby, we propose a two-level gradient heterogenous nanograined structure for overcoming the strength-ductility trade-off of the FeCoNi MEA and successfully fabricate a large-scale ultrastrong gradient bulk nanograined FeCoNi MEA using Ultrasonic assisted Cyclic Thermal-dynamic Solid-state physical processes (UltraCTS). Fig. 1 (a) illustrates the scheme of the proposed solid-state materials processing method. High frequency ultrasonic signal provides the vibration of the ultrasonic tip. High strength steel shots with the diameter of 1∼5 mm placed on the surface of the tip will be accelerated by the high frequency vibration and impact the target surface with high velocities and high frequency. Then, the shots will be rebounded back to the vibrating surface and change their directions to impact the target materials again. Cyclic severe plastic strain $\Delta\varepsilon^p$ will be introduced into the target surface by the high-speed shots efficiently as illustrated in Fig. 1 (b). The strength of the target surface will be enhanced by this cyclic plastic strain accumulation due to the strain hardening and grain refinement process as illustrated in Fig. 1 (c). Severe plastic deformation can be effectively introduced in the target surface as illustrated in the inset of Fig. 1(c). One of the advantages of this technology is that we can get gradient heterogenous nanograined structure on the target materials, allowing us to study the mechanical responses of the nanocrystalline and single crystalline MEA on one sample to eliminate the experimental errors due to sample preparation. On the gradient heterogenous nanograined sample, micropillars with *nanocrystalline* and *single crystalline* microstructure are fabricated from the top surface of the sample and matrix materials, respectively as illustrated in Fig. 1 (d) and (e). The insets of Fig. 1 (a) illustrate the plane-view, cross-sectional view of the as-fabricated sample and the locations of the micropillars. Furthermore, it is known that the mechanical strength and ductility of the materials can be enhanced by developing a gradient NC layer on its outmost surface. According to Fang et al., the gradient NC structure can perfectly evade the trade-off between the strength and ductility of the metal and alloys. They developed a gradient NC film on the coarse-grained copper substrate with a gradient transition of grain size. The gradient NC copper film exhibits a 10 times higher yield strength compared to that of the coarse-grained substrate and can sustain a tensile true strain exceeding 100% without failure [28]. Additionally, the improved fatigue life of the components with gradient NC layer has also been demonstrated in the recently published literatures [29–32]. Hence, it is promising to develop high performance FeCoNi MEA components by developing an ultrastrong gradient heterogenous nanograined structure on their outermost surface. This ultrastrong gradient heterogenous nanograined structure can act as an "armor" to protect the matrix core materials from crack and failure due to its ultrahigh yield strength, typically several times higher than that of the matrix materials. Another advantage of this cyclic thermal-dynamic solid-state physical processing technology comparing to other mechanical strengthening/SPD methods, e.g. rolling, HPT et al., is that the cyclic plastic strain allows the materials have time to nucleate and recrystallize, which results in stable nanostructure for finer grain size. The inset of Fig. 1 (d) illustrates the magnified characterizations of the as-fabricated NC FeCoNi micropillar and the extremely fined nanograins (10–20 nm) marked by the red arrows can be clearly identified. Detailed materials characterizations of the gradient heterogenous nanograined structure will be illustrated in the following sessions. In summary, we demonstrate an efficient method to get a two-level heterogeneous nanograined structure for overcoming the strength-ductility trade-off of the FeCoNi MEA. The first-level heterogenous structure is the nanocrystalline surface layer with the grain size varying from 10 to 200 nm located at the topmost surface of the FeCoNi MEA as illustrated in Fig. 1 (d). The extremely fined nanograins (10–50 nm) can make the materials/micropillar superb strong and stable [33,34], while the ultrafine grains (50–200 nm) can act as the sources of the dislocations resulting reasonable ductility. The second-level heterogenous structure is the gradient nanograined layer with the thickness of up to 500 μm as illustrated in Fig. 1 (c). This gradient heterogenous nanocrystalline structure along the cross-sectional direction of the metal and alloys has been proved to be an effective structure to overcome strength-ductility

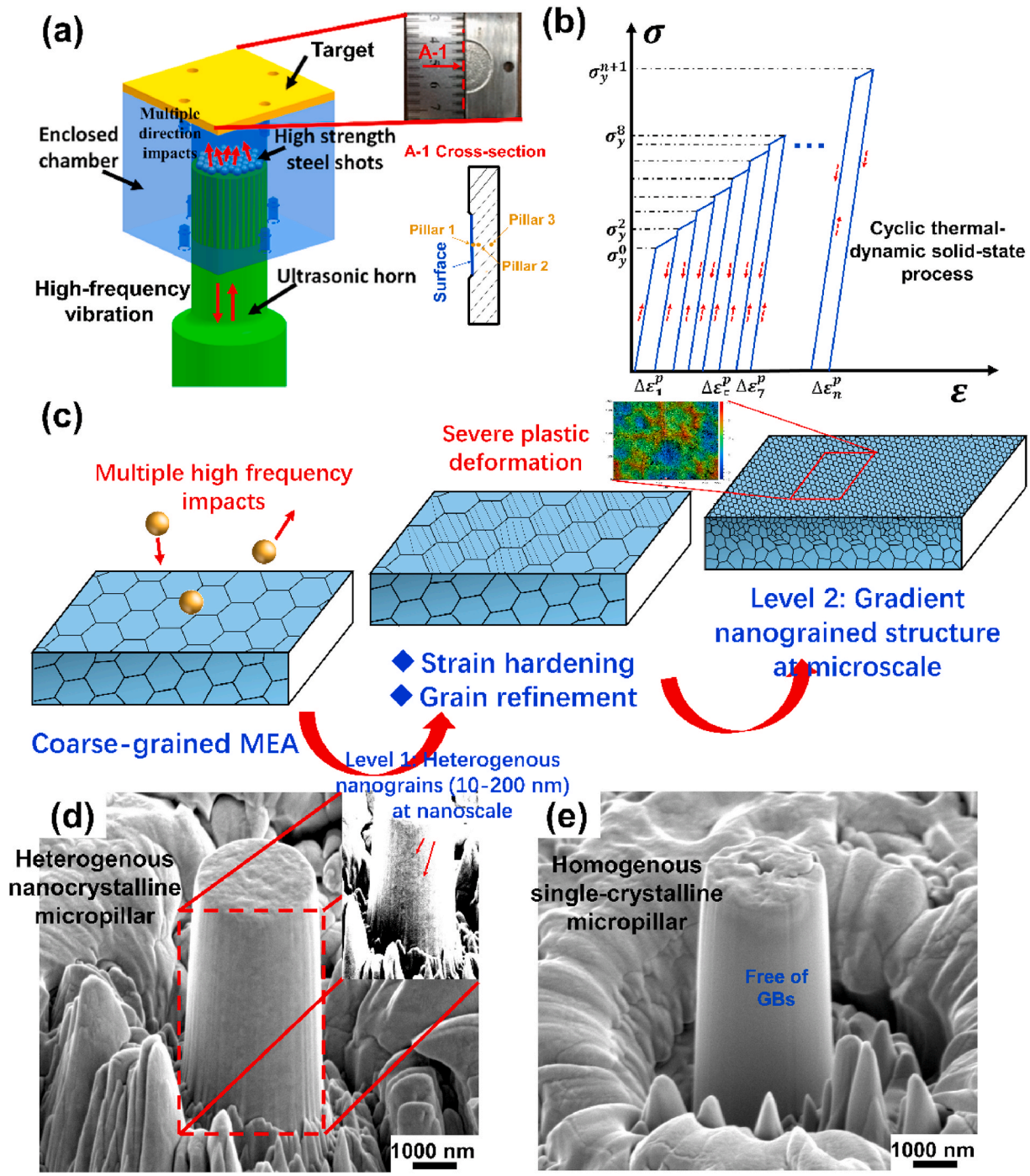

Fig. 1. (a) Scheme of the ultrasonic assisted cyclical thermal-dynamic solid-state physical process; (b) mechanical strengthening of the MEA during the cyclic thermal-dynamic solid-state physical process due to the accumulated plastic strain; (c) Scheme of the grain refinement process of the MEA via the ultrasonic assisted cyclic thermal dynamic solid-state physical process and (d) a nanocrystalline micropillar with high density dislocation and grain boundary and (e) a single crystalline micropillar free of grain boundary. (The micropillars are captured via SEM with a stage tilt of 52°).

of the metal and alloys at macroscale [27,35,36]. The two-level heterogeneous nanograined structure of the developed FeCoNi MEA could make it ultrastrong and ductile at multiple length scales.

2. Materials and methods

The equiatomic FeCoNi medium entropy alloy (MEA) is produced by melting the element Fe, Co and Ni (>99.9% pure) in a 25 kg vacuum induction furnace. The diameter of the as-cast ingot is 120 mm. To eliminate the element segregation of the cast, the ingot is homogenized for 15 h at the temperature of 1473 K. Then, it is rolled at the temperature of 1503 K and the final diameter of the cast is 60 mm. The ultrasonic assisted cyclic thermal-dynamic solid-state physical processes as illustrated in Fig. 1 is used to get large-scale NC FeCoNi MEA. In this study, high-strength steel balls with the dimeter of 3 mm are used to impact the target surface repeatedly within an enclosed chamber. The frequency of the ultrasonic vibration is 20 KHz. After the treatment, the sample is cut from the cross-sectional direction and polished by the sandpapers and diamond paste to get a mirror-like surface. It should be clarified that all the mechanical tests are done at different depths

separately from the cross-section of the sample. Focused Ion Beam (FIB) is used to prepare a TEM sample from the treated sample at the topmost surface by using the FEI QUNTA 3D FIB/SEM dual beam system. The width and length of the TEM lamellar is 6 μm and 10 μm, respectively. The TEM sample is then characterized by the FEI Talos 200X with the accelerating voltage of 200 kV. The HAADF-STEM EDS scanning of the NC FeCoNi MEA is used to characterize the element segregation and/or second phase formation at nanoscale. To get the mechanical behaviors of the NC FeCoNi MEA at different length scales from nanometers to micrometers, nanohardness and Young's modulus of the gradient NC FeCoNi MEA are measured using the Agilent Nanoindenter G200 equipped with the Berkvich tip. A series of the indent sites are selected along the cross-sectional direction of the sample. The distance between each indent site is set as 5 μm. The maximum displacement of the tip during the tests is set as 1000 nm and the strain rate is set as 0.05 s^{-1} with a maximum allowable drift rate of 0.05 nm/s. To get the flow stress and strain hardening exponent of the NC FeCoNi MEA at different length scales, micropillars are fabricated on the gradient NC FeCoNi HEA alloy using the FIB/SEM system. The grain structure of the micropillars is controlled by precisely controlling their locations on the gradient NC MEA sample. In this study, the nanocrystalline micropillars are fabricated at the location of 2 μm and 5 μm depth from the topmost surface, respectively. A single crystalline micropillar is fabricated from the coarse-grained matrix materials. The diameter and height of the micropillar is 3 μm and 6 μm, respectively. To guarantee the surface quality of the micropillars, all the micropillars are finally polished using the ion current of 10 pA in the FIB/SEM system. The as-fabricated micropillars are compressed by using the Agilent Nanoindenter G200 with a flat diameter tip at the strain rate of 0.05 s^{-1}. The SEM characterizations are conducted to observe the microstructure of the micropillars before and after the compression tests. The dimension of the micropillars before the compression tests is carefully measured in the SEM system for the strain and stress calculation. Strain rate sensitivity (SRS) for the FeCoNi MEA at multiple length scales is measured by using the continuous-stiffness-measurement (CSM) strain-rate jump test methods described by Maier et al. [37]. The maximum and minimum strain rate during the tests are set as 0.1s^{-1} and 0.0001 s^{-1}, respectively.

3. Results

3.1. Two-level heterogenous nanograined structure

Fig. 2 illustrates the TEM characterizations of the gradient heterogenous nanocrystalline (NC) FeCoNi MEA at different locations along the cross-sectional direction. It should be noted that because of the gradient plastic strain along the cross-sectional direction of the sample during the grain refinement process, a gradient NC structure is supposed to be fabricated. Fig. S1 illustrates the EDX mapping of the as-fabricated NC MEA at nanoscale. It can be seen in Fig. S1 that the materials are still the FeCoNi alloy and there is no nano-precipitates in the NC layer. Fig. 2 (a)–(c) illustrates the bright field (BF), dark field (DF) and selected area diffraction pattern (SADP) of the NC FeCoNi HEA at the topmost surface. The equiaxed nanograins have been successfully fabricated and marked by the red arrows in Fig. 2 (a). Extremely fined nanograins with the size of 10–20 nm is characterized and marked in Fig. 2 (b). The diffraction ring marked in Fig. 2 (c) confirms the formation of the randomly

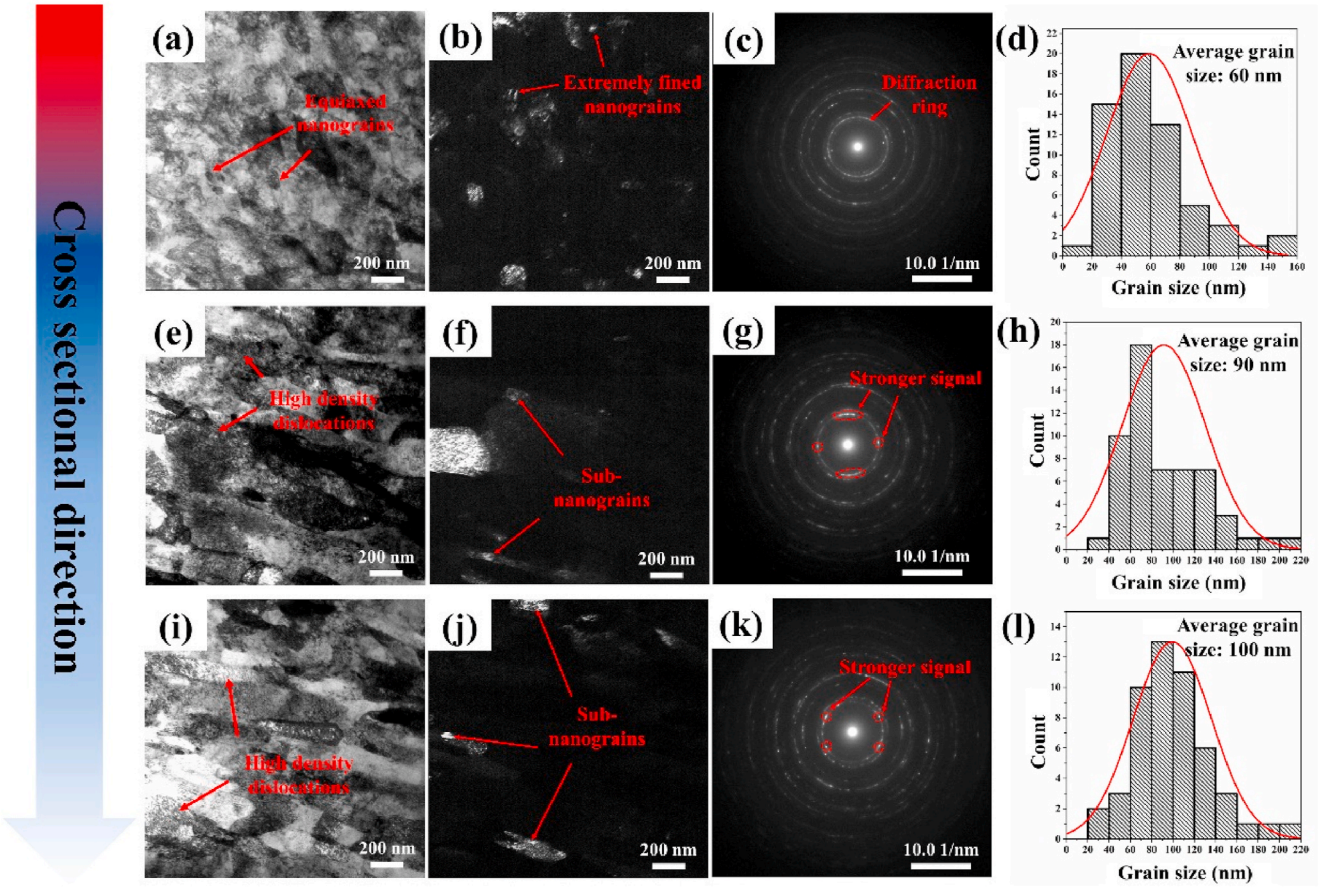

Fig. 2. TEM characterizations of the gradient heterogenous nanograined FeCoNi medium entropy alloy (MEA) along the cross-sectional direction: (a) bright field (BF), (b) dark field (DF), (c) selected area diffraction pattern (SADP) and (d) statistical analysis of the grain size for the NC FeCoNi MEA at the location of 2 μm depth from the treated surface; (e) BF, (f) DF, (g) SADP and (h) statistical analysis of the grain size for the NC FeCoNi MEA at the location of 6 μm depth from the treated surface; (i) BF, (j) DF, (k) SADP and (l) statistical analysis of the grain size for the NC FeCoNi MEA at the location of 10 μm depth from the treated surface.

oriented equiaxed nanograins at this location. The grain size of the FeCoNi MEA varies from 10 nm to 220 nm according to the statistically analysis illustrated in Fig. 2 (d), indicating heterogeneous nanograined structure of the FeCoNi MEA is obtained at nanoscale; Fig. 2 (e)–(g) illustrate the BF, DF and SADP of the NC FeCoNi MEA at the location of 6 μm depth from the topmost surface. It can be seen in Fig. 2 (e) that the lath-shaped grains are fabricated at this depth and some tiny equiaxed nanograins distribute between the lath-shaped grains. High-density dislocation is marked in Fig. 2 (e). Fig. 2 (f) shows the DF characterization of this area. The sub-nanograins can be identified in Fig. 2 (f) and marked by the red arrows. Stronger signal points circled in Fig. 2 (g) indicate orientated nanograins, which is consistent with the BF characterization in Fig. 2 (e). Fig. 2 (i)–(k) illustrate the BF, DF and SADP of the NC FeCoNi MEA at the location of 10 μm depth from the topmost surface. We can identify lath-shaped nanograins and sub-grains at this area as well. High density dislocation can be seen in Fig. 2 (i) and there are some stronger signal points as indicated in Fig. 2 (f), indicating orientated nanograins have been fabricated. Fig. 2 (d), (h) and (i) illustrate the statistically analysis of the grain structure of the gradient heterogenous nanograined MEA. The average grain size of this gradient heterogenous nanograined FeCoNi MEA at the location of 2 μm, 6 μm and 10 μm depth from the topmost surface is 60 nm, 90 nm and 100 nm, respectively. With the increase of the distance from the topmost surface, the average grain size of the gradient heterogeneous nanograined FeCoNi MEA increases gradually. This gradient characteristic structure agrees well with the gradient nanograined structure fabricated on the stainless steel [38], low carbon steel [39] and copper [40] et al. reported in our previously published studies. It should be noted that the gradient transition of the grain size in the NC MEA layer is not significant along the depth.

The extremely fined nanograined (ex-NG) structure defined as the grain size that less than 20 nm can be identified in Fig. 2 (a) and (b). Nanograined (NG) structure defined as the grain size that less than 100 nm and the ultrafine grained (UFG) structure defined as the grain size that less than 1000 nm can be characterized in the gradient nanograined surface layer as illustrated in Fig. 2 as well. The extremely fined nanograins with the grain size of 10–20 nm contribute to the superb strength and stability of the heterogenous structure, while the NG and UFG with the grain size from 20 to 200 nm characterized in Figs. 1 (d) and Fig. 2 (a) can ack as the dislocation source of the heterogenous materials during the plastic deformation. The level 1 heterogeneous structure of the materials possess reasonable strength and ductility at nanoscale. The gradient heterogeneous nanograined structure makes the entire MEA component strong and ductile at macroscale, which is defined as the level-2 heterogenous strengthening mechanism hereby.

3.2. Nanohardness and modulus

Fig. 3 illustrates the distribution of the nanohardness and Young's modulus of the gradient heterogenous nanograined FeCoNi MEA along the cross-sectional direction from the top surface to the matrix core materials. The nanohardness decreases gradually with the increase of the depth from the topmost surface. And the hardest material locates at the topmost surface with the nanohardness value of 4.92 GPa. There is a sharp nanohardness gradient at the top surface of the sample with the layer thickness of around 150 μm. This test result is consistent with the gradient NC structure as characterized in Fig. 2 and can be explained by using the Hall-Petch grain boundary strengthening mechanism. Fig. 3 also illustrates the distribution of the Young's modulus of the gradient NC MEA alloy along the cross-sectional direction. We found that there is no significant change of the Young's modulus of the gradient NC FeCoNi MEA. And the Young's modulus of the FeCoNi MEA is 177.7± 9 GPa, which agrees well with the results presented by Laplanche et al. [10]. They indicated that the modulus of the FeCoNi MEA is 175 MPa.

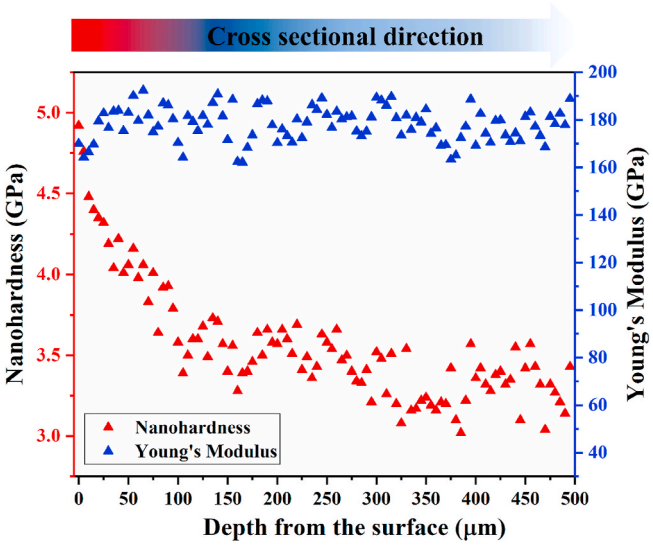

Fig. 3. The nanohardness and Young's modulus of the gradient NC FeCoNi MEA along the cross-sectional direction from top surface to the matrix core materials.

3.3. Micropillar compression test

Fig. 4 (a) illustrates the engineering stress-strain of the heterogenous nanocrystalline (NC) micropillar with the average grain size of 60 nm and 90 nm and the single crystalline (SC) micropillar free of grain boundaries. The grain size in the micropillars is determined by precisely controlling the location of the micropillars on the sample. Firstly, a significantly improvement of the yield strength for the heterogenous NC micropillar is achieved comparing to its SC counterpart. The tested yield strength of the SC micropillar is around 375 MPa, which is much higher than the data obtained from the tensile test, 190 MPa, reported by Wu et al. [17]. Size effect should be taken into consideration for the SC micropillar compression. The average grain size (less than 100 nm) in the NC micropillar is much smaller than the dimension of the micropillar with the diameter and height of 3000 nm and 6000 nm, respectively. Hence, the size effect for the NC micropillars can be ignored. The yield strength of the heterogenous NC micropillar with the average grain size of 60 nm and 90 nm is 1.48 GPa and 1.12 GPa, respectively. And the ultimate strength of the NC micropillar can reach as high as 1.7 GPa. The yield strength of the NC MEA developed in this study is almost 8 times higher than that of coarse-grained MEA. One thing should be noted is that the developed heterogenous NC MEA exhibits a ductility of 45% (60 nm NC micropillar) and >25% (90 nm NC micropillar) in compression at ambient temperature, respectively, which indicates that the developed heterogenous NC MEA has a reasonable formability at microscale. Secondly, we find stress avalanches in the engineering stress-strain curve of the SC micropillar as indicated in Fig. 4 (a). This phenomenon has also been observed in other materials system, such as 316L stainless steel [38,41]. When the SC micropillar is deformed, dislocations will move directly to the surface of the micropillar and vanish suddenly due to the lack of grain boundaries. The sudden vanish of the dislocation generates multi-direction slip bands on the surface of the deformed SC micropillar as illustrated in Fig. 4 (d). In contrast, there are no slip bands on the deformed NC micropillars as illustrated in Fig. 4 (c) and (b). Instead, deformation wrinkles are observed in the NC micropillars. That's because when the NC micropillars are deformed, dislocation movements are hindered by the high-density grain boundaries at nanoscale. Thirdly, according to the micropillar compression test results, the mechanical strength of the FeCoNi MEA can be significantly improved by (a) the transition from SC structure to the NC structure, (b) Hall-Petch effect and (c) strain hardening as illustrated in Fig. 4 (a). We

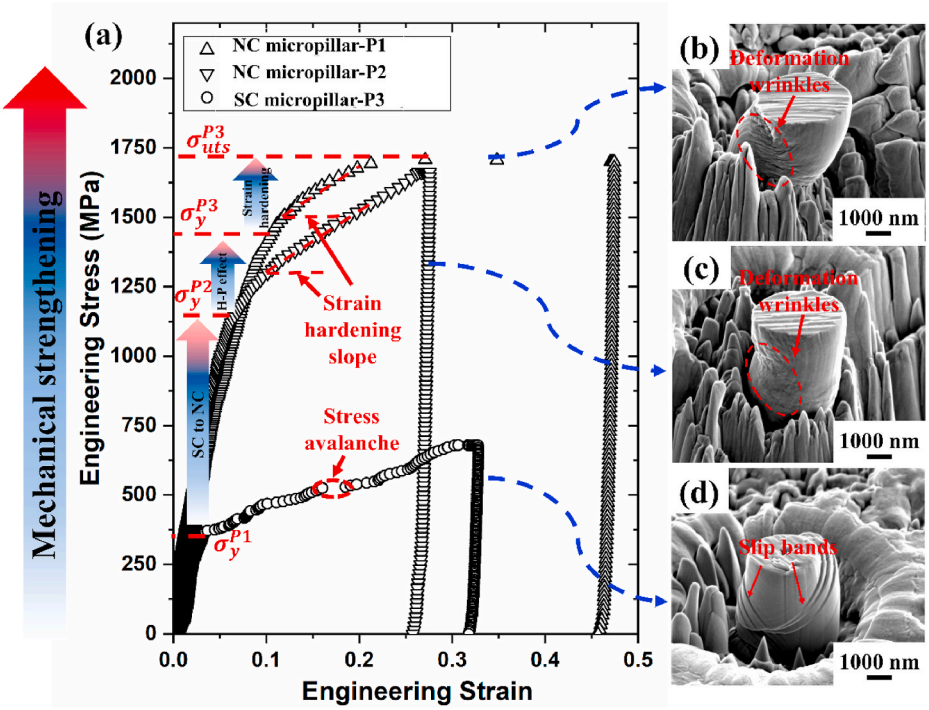

Fig. 4. (a) Engineering stress-strain curves of the NC FeCoNi MEA with the average grain size of 60 nm and 90 nm and the engineering stress-strain curve of the signal crystalline FeCoNi MEA. The deformed micropillar at the locations of (b) 1.5 μm, (c) 6 μm and (d) 1500 μm depth from the topmost surface on the NC FeCoNi MEA sample. (All the SEM pictures were captured in the same magnification with a tilt angle of 52°).

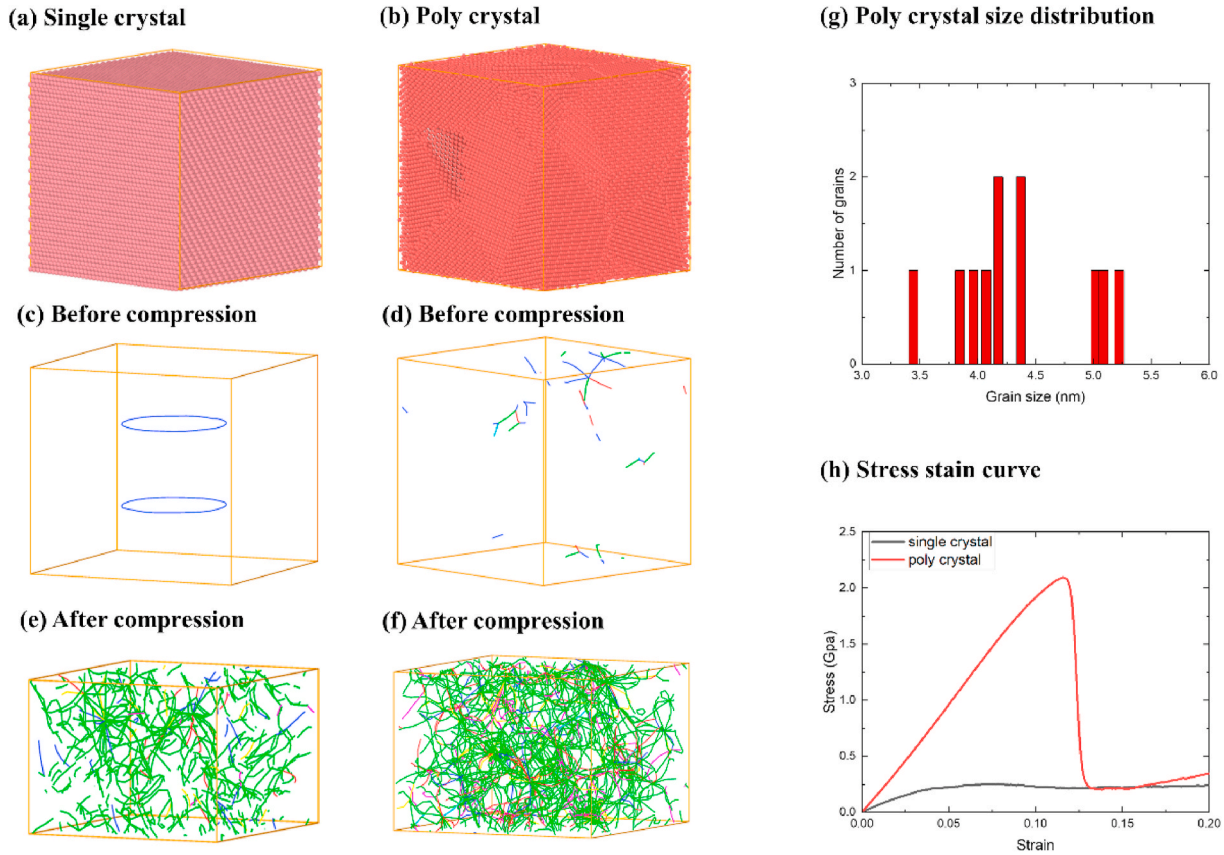

Fig. 5. MD simulation for compression of FeCoNi medium entropy alloy. a)~f) Atomic model and dislocation distribution before and after compression for single crystal and poly crystal respectfully. g) grain size distribution for the poly crystal model. h) stress strain curves after compression.

will discuss and quantify these strengthening mechanisms later.

In this study, the Large-scale Atomic/Molecular Massively Parallel Simulator (LAMMPS) was used for MD simulation of compression for single and poly crystal FeCoNi medium entropy alloy. Atomic configuration for the models were shown in Fig. 5 (a) and (b) for single crystal and poly crystal respectfully. Dimension of the simulation box was about 10 *10*10 nm^3. Grain size for the poly crystal model was between 3 nm–6 nm and its distribution was demonstrated in Figure (g). Before compression, initial dislocations with density around 3*1012/cm^2 were introduced in the model to account for the plastic deformation during shot peening process. The embedded atom model potential (EAM) was used to compute pairwise interactions among Fe–Co–Ni atoms. The systems were equilibrated at 300 K and zero pressure using the constant temperature and pressure ensemble (NPT) for 2 ns with a time step 1 fs. During compression loading, strain rate along the z direction was 1 * 1010 s^{-1} with periodic boundary conditions for x- y- and z-directions. MD simulation results were showed in Fig. 5 (e) and (f) for single and poly crystal after compression. And OVITO was used for visualization the dislocation structures. Stress strain curves were presented in Fig. 5 (h). For single crystal, its yield strength was around 250 Mpa. While poly crystal had much higher strength around 2.1 GPa. The results agree with the experimental results illustrated in Fig. 4.

4. Discussion

4.1. Strengthening mechanism

The acknowledged Hall-Petch relationship as shown in equation (1) is used to describe the grain refinement strengthening phenomenon of this gradient heterogeneous nanograined FeCoNi MEA.

$$\sigma_y = \sigma_0 + K_y d^{-1/2} \quad (1)$$

where, σ_y is the yield strength of the MEA; d is the average grain size of the materials; σ_0 is the friction stress and K_y is a yield constant.

According to Wu et al., the yield strength of the coarse grained FeCoNi MEA with the grain size of 28 μm is 190 MPa [17]. Additionally, Yoshida et al. [42] developed the Hall-Petch equation for the FeCoNi MEA at microscale. They stated that the developed Hall-Petch equation can be used to describe the relationship between the yield strength of the FeCoNi MEA and its average grain size at microscale. However, it is still a challenge to develop Hall-Petch equation of the FeCoNi MEA at nanoscale because of the lack of the materials data. Due to the higher stacking fault energy of FeCoNi MEA, it is more difficult to get nanosized grains (<100 nm) than other Fe–Co–Cr–Mn–Ni HEAs/MEAs via conventional severely plastic deformation method, such like the high-pressure torsion (HPT). The finest grain size for the FeCoNi MEA obtained from HPT reported by Yoshida is 5.64 μm. In this study, we successfully get gradient heterogeneous nanograined structure on the FeCoNi MEA and measure the mechanical strength of the FeCoNi MEA. By using the data reported by Wu et al. as well as Yoshida et al., and the data obtained in this study, we develop the Hall-Petch relationship for the FeCoNi MEA from coarse-grained regime to nanograined regime as shown in Equation (2) and Fig. 5 (a).

$$\sigma_y = 81.02 + 10485.5 * d^{-1/2} \quad (2)$$

where, σ_y is the yield strength of the FeCoNi MEA and d is the average grain size of the FeCoNi MEA with the unit of nanometer.

Fig. 6 (a) illustrates the Hall-Petch plot of the FeCoNi MEA at multiple length scales from coarse-grained to nanograined regime. The strength of the FeCoNi MEA at nanoscale can be precisely tuned by controlling the grain structure of the materials. It is the first time according to the authors' knowledge that precisely Hall-Petch equation for FeCoNi MEA is reported and verified at nanoscale. It should be noted that we used compression tests to measure the yield strength of the NC MEA at microscale due to the limitation of the micro-tensile equipment. The finest grain size of the NC MEA developed in this study is 60 nm as illustrated in Fig. 2. Hall-Petch strengthening mechanism still works in this length scale and can be used to develop a universal linear equation at different length scales. All the micropillars were fabricated from a cross-sectional NC MEA sample and there is no gradient of the grain structure along its height. Hence, the yield strength of the micropillars measured from the compression tests can be used to develop the H–P strengthening equation for the FeCoNi MEA at multiple length scale. This mathematical relationship can be used in the strength tolerance design and grain refinement for high performance NC MEA component in the future applications. Fig. 6 (b) illustrates the comparison of the developed high strength NC FeCoNi MEA with other coarse-grained and nanograined HEAs/MEAs from the aspects of yield strength and plastic strain to failure. Currently, study on the nanograined HEAs/MEAs is insufficient and research on this topic is emerging because the mechanical behaviors and deformation mechanism of the HEAs/MEAs at nanoscale are still unclear [43]. We summary and collect the experimental data of the coarse-grained (CG), ultrafine-grained (UFG) and nanograined (NG) FCC Fe–Co–Cr–Mn–Ni system as shown in Table 1 and

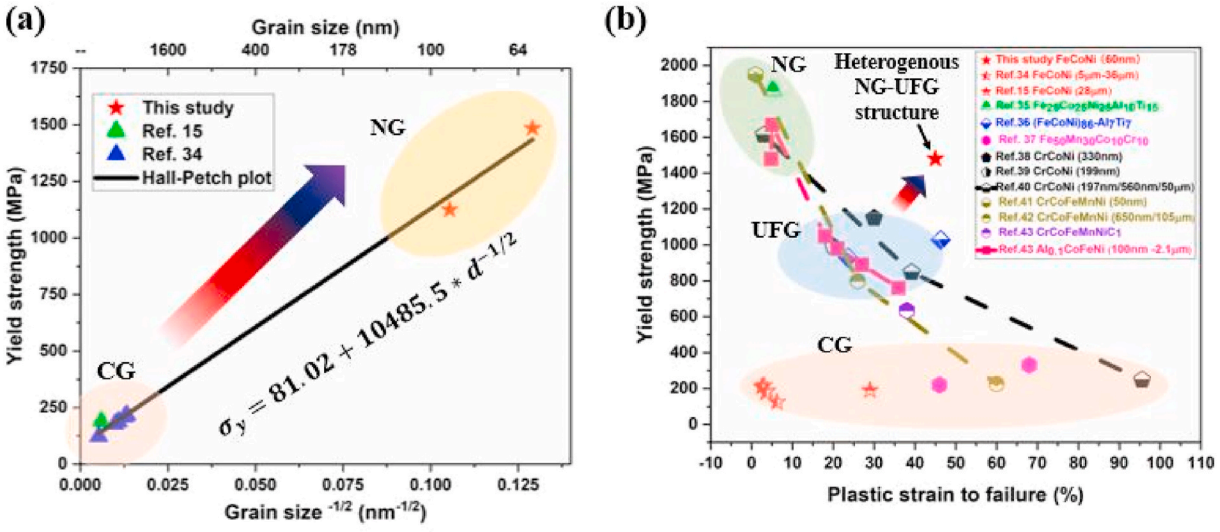

Fig. 6. (a) Hall-Petch relationship of the FeCoNi MEA at multiple length scales from nanometer to micrometer regime and (b) comparison of the NC MEA developed in this study with other FCC HEAs/MEAs with coarse-grained (CG), ultrafine-grained (UFG) and nanograined (NG) structure, data are derived from the references.

Table 1
Mechanical strength of the FCC Co–Cr–Fe–Mn–Ni system HEAs/MEAs with coarse-grained (CG), ultrafine-grained (UFG) and nanograined (NG) structure obtained from this study and reported by the published literatures.

Materials	Grain size	$\sigma_y/\sigma_{0.2}$ (MPa)	σ_{UTS} (MPa)	Plastic strain to failure (%)	Method	Phase condition	Ref.
FeCoNi	60 nm	1480	1750	~20%	UltraCTS	–	This study
FeCoNi	90 nm	1120	1730	~27%	UltraCTS	–	This study
FeCoNi	5.64 μm	216.71		3%	HPT + annealing	FCC	[42]
FeCoNi	6.26 μm	208.88	–	2.5%	HPT + annealing	FCC	[42]
FeCoNi	8.41 μm	188.81	–	3.9%	HPT + annealing	FCC	[42]
FeCoNi	10.2 μm	177.20	–	3.5%	HPT + annealing	FCC	[42]
FeCoNi	36.4 μm	123.26	–	6.2%	HPT + annealing	FCC	[42]
FeCoNi	28 μm	190	500	29%	CR + annealing	FCC	[17]
$Fe_{25}Co_{25}Ni_{25}Al_{10}Ti_{15}$	FCC 227 nm; BCC 409 nm	1860	2520	5.2%	MA + SPS	82.3%FCC+17.7%BCC+ γ' nanoprecipitates	[18]
$(FeCoNi)_{86}$–Al_7Ti_7	–	1028 ± 6	1446 ± 18	46.3 ± 2.2	Arc melting + water quenching + CR + Aging	FCC + $L1_2$	[19]
$(FeCoNi)_{86}$–Al_8Ti_6	–	930 ± 4	1267 ± 4	23.6 ± 0.6	Arc melting + water quenching + CR + Aging	FCC + $L1_2$	[19]
$Fe_{50}Mn_{30}Co_{10}Cr_{10}$	45 μm	220	710	46	HT + Water quenching + CR + Annealing	FCC + HCP	[20]
$Fe_{50}Mn_{30}Co_{10}Cr_{10}$	4.5 μm	330	880	68%	HT + Water quenching + CR + Annealing	FCC + HCP	[20]
CrCoNi	330 nm	1150	–	30%	CR + Annealing	FCC	[47]
CrCoNi	199 nm	993	–	~20%	HPT + Annealing	FCC	[48]
CrCoNi	197 nm	1613.2	1741.3	3%	CR90%	FCC	[49]
CrCoNi	50 μm	248	740	95.6%	CR90%+Annealing(1373K/1h)	FCC	[49]
CrCoNi	560 nm	848	1087.7	39.2%	CR90%+Annealing(973K/1h)	FCC	[49]
CrCoFeMnNi	50 nm	1950	–	Very low, Not given	HPT	FCC	[44]
CrCoFeMnNi	105 μm	225±3	557±5	60±4%	CR + Annealing	FCC	[45]
CrCoFeMnNi	650 nm	798±13	887±16	26±1	CR + Annealing	FCC	[45]
$CrCoFeMnNiC_1$	5 μm	634	843	38%	CR + Annealing	FCC + $M_{23}C_6$	[50]
$Al_{0.1}$CoCrFeNi	–	1480	~1480	4.8%	Cryo-rolling	FCC	[46]
$Al_{0.1}$CoCrFeNi	100 nm	1670	~1670	5%	Cryo-rolling + Annealing	FCC	[46]
$Al_{0.1}$CoCrFeNi	900 nm	1050	~1030	18%	Cryo-rolling + Annealing	FCC	[46]
$Al_{0.1}$CoCrFeNi	1.1 μm	980	~1000	21%	Cryo-rolling + Annealing	FCC	[46]
$Al_{0.1}$CoCrFeNi	1.3 μm	890	~955	27%	Cryo-rolling + Annealing	FCC	[46]
$Al_{0.1}$CoCrFeNi	2.1 μm	760	~870	36%	Cryo-rolling + Annealing	FCC	[46]

UltraCTS: Ultrasonic assisted cyclic thermal dynamic solid-state physical process; HTP: High Pressure Torsion; CR: Cold Rolling; MA: Mechanical Alloying; SPS: Spark Plasma Sintering; HT: Hot Rolling.

illustrate the data in Fig. 6 (b). The mechanical strength of the HEAs/-MEAs can be significantly enhanced by decreasing the average grain size of the materials according the golden, pink, and black dash lines for the CrCoFeMnNi [44,45], $Al_{0.1}$CoFeNi [46] and CrCoNi [47–49] illustrated in Fig. 6 (b). The plastic strain to failure of these materials decreases significantly and these "banana shape" curves implying strength-ductility trade-off phenomenon is consistent with the conventional NG metal and alloys found in the stainless steel, nickel and copper et al. Surprisingly, the developed heterogenous nanograined FeCoNi MEA in this study exhibits a yield strength of 1.48 GPa and a ductility of 45% in compression at microscale as illustrated in Figs. 4 and 5 (b). Yang et al. pointed out that the sustainable strain hardening rate of the materials can benefit the ductility of the materials. They developed a heterogenous grain structure (HGS) with grain sizes spanning the nanometer to micrometer range via partial recrystallization annealing following conventional coral rolling of CrCoNi MEA. And the as-fabricated HGS CrCoNi MEA exhibits a high yield strength of 1.0 GPa and a uniform tensile strain of 22% [47]. We believe the superb ductility of the developed heterogenous nanograined FeCoNi MEA is originated from the pronounced work-hardening rates illustrated in Fig. 4 (a). It can be seen in Fig. 4 (a) that the strength of the heterogenous nanograined FeCoNi MEA is work hardened from 1.48 GPa to 1.7 GPa, implying high density grain boundaries at nanoscale and the heterogenous nanograined structure spanning from 10 nm to 200 nm can lead to a sustainable strain hardening rate when the materials is deformed at microscale.

4.2. Strain rate sensitivity

Strain rate sensitivity (SRS) of the metal and alloys at nanoscale is emerging because it can imply the deformation mechanisms of the nanograined metal and alloys [51,52]. However, SRS exponent for the FeCoNi MEA at nanoscale is still unknown. The ultrastrong gradient nanocrystalline FeCoNi MEA fabricated in this study provides the authors a research window to conduct symmetrical study of the SRS exponent of the materials from nanoscale to microscale. Fig. 7 illustrates the investigation on the SRS of the gradient NC MEA at multiple length scales by controlling the locations of strain rate jump test using nanoindentation. Strain rate jump test method using nanoindentation has been proved to be an effective test method to get the SRS of the metal and alloys at nanoscale [37,53]. Fig. 7 (a) illustrates the load-displacement curves of the tests with the strain rates of 0.1 s^{-1}, 0.018 s^{-1}, 0.003 s^{-1}, 0.001 s^{-1} and 0.0001 s^{-1} for the nanograined (NG), ultrafine grained (UFG) and coarse-grained (CG) FeCoNi MEA, respectively. It can be seen in Fig. 7 (a) that there are stress pop-ins during the tests for the NG-MEA, UFG-MEA and CG-MEA. The load on the NG-MEA sample is higher than that on the UFG-MEA and CG-MEA. Fig. 7 (b) illustrates the tested nanohardness for the NG-MEA, UFG-MEA and CG-MEA with different strain rates. Using the tested nanohardness with different strain rates, the strain rate sensitivity exponent can be calculated by the following equation [37]:

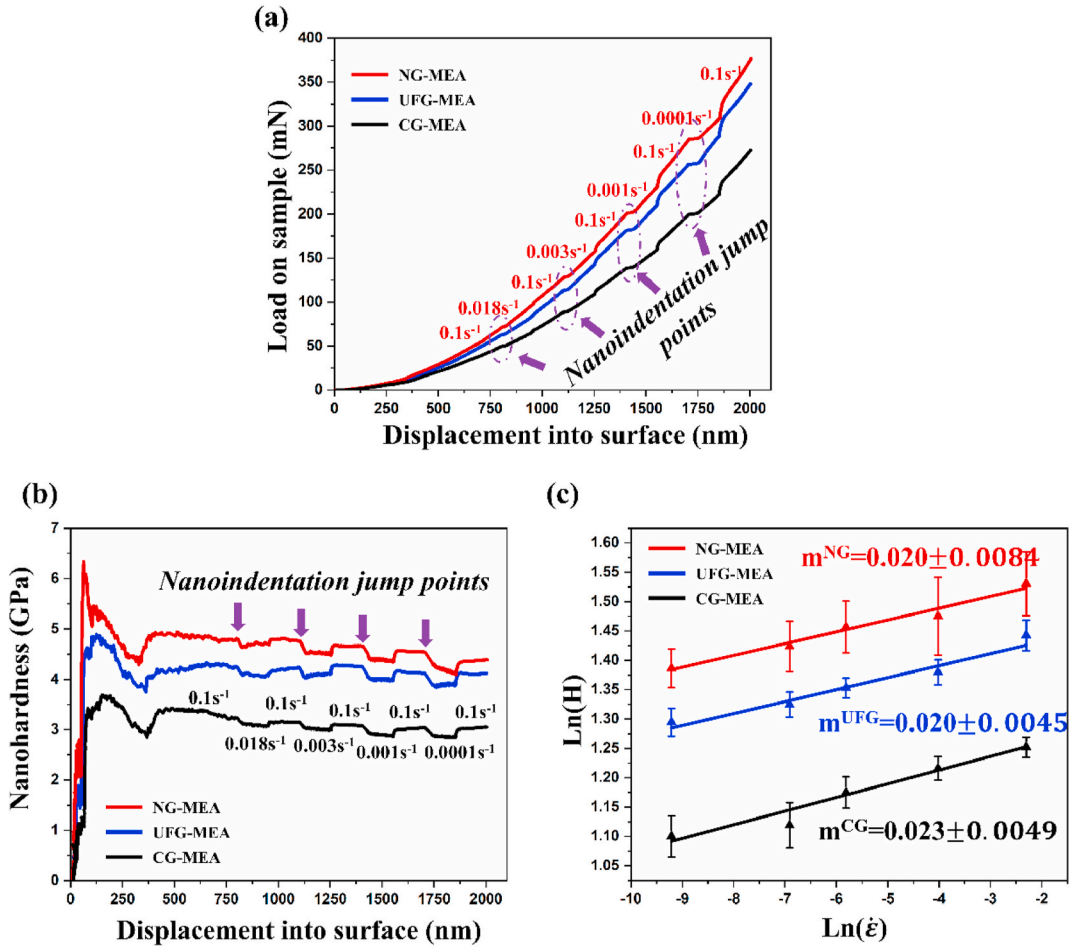

Fig. 7. (a) The load-displacement curves of the strain rate jump nanoindentation tests on the gradient NC FeCoNi MEA at multiple length scales; (b) The nanohardness of the gradient NC FeCoNi MEA with respect to the displacement and (c) the strain rate sensitivity of the gradient NC FeCoNi MEA from nanograined structure to coarse-grained matrix material.

$$m = \frac{d(ln\sigma_y)}{d(ln\dot{\varepsilon})} \tag{3}$$

where, m is the SRS exponent, which describes the SRS behavior of the materials assuming a constant microstructure, σ_y is the yield strength of the materials and $\dot{\varepsilon}$ is the strain rate during the test. It can be seen in Fig. 6 (c) that the SRS exponent of the NG-MEA, UFG-MEA and CG-MEA is 0.020±0.0084, 0.020±0.0045 and 0.023±0.0049, respectively. The test results indicate that there is no significant change of the SRS for the MEA with different grain structure. This data can be used to describe the rate-dependent behavior of the FeCoNi MEA during the plastic deformation at multiple length scales.

It should be noted that the SRS exponent is dependent on the grain size for most conventional metallic materials. For example, Yin et al. studied the strain rate sensitivity of the nanocrystalline 316L stainless steel and they found that there is a significant decrease of the SRS exponent for the NC 316L stainless steel with the average grain size of 5 nm [51]. And the increase of the SRS exponent value has been observed in the FCC metals such as copper [54–56], Ni [57] and Au [58], while the reduction of the SRS exponent value is reported in the BCC metals such as Fe [59–61], Ta [62], and V [63]. For the high/medium entropy alloys, the lattice distortion could make the materials posse different deformation mechanism at nanoscale. Equation (4) describes the flow stress of the MEA during the plastic deformation. The mechanical strength of the MEA includes the Hall-Petch effect, solution strengthening and strain hardening as formulated in equation (4).

$$\sigma(\dot{\varepsilon}, \varepsilon_p, d, T) = \sigma_{HP}(d) + \sigma_{ss}(T, \dot{\varepsilon}) + \sigma_f(T, \varepsilon_p, d) \tag{4}$$

where, $\dot{\varepsilon}$ is the strain rate, ε_p denotes the plastic strain, d is the grain size of the materials and T is the working temperature. σ_{HP} is the Hall-Petch strength; σ_{ss} is solution strength and σ_f is flow stress. In this study, the MEA is deformed at room temperature and we are only focusing on the yield strength of the MEA. Hence, equation (4) can be simplified into equations (5) and (6).

$$\sigma(\dot{\varepsilon}, \varepsilon_p, d)_{at\ RT} = \sigma_{HP}(d) + \sigma_{ss}(\dot{\varepsilon}) + \sigma_f(\varepsilon_p, d) \tag{5}$$

$$\sigma_Y(\dot{\varepsilon}, d)_{at\ RT} = \sigma_{HP}(d) + \sigma_{ss}(\dot{\varepsilon}) \tag{6}$$

where, σ_Y is the yield strength of the MEA. In equation (8), σ_{HP} is only depend on the average grain size d of the MEA, which has been formulated in equation (2). Solution strength is the second portion of the yield strength of the MEA and it depends only on the strain rate [64]. A materials model developed by Varvenne et al. is utilized to describe the solution strengthening of the MEA [65] as shown in equations (7)–(9).

$$\sigma_{ss}(T, \dot{\varepsilon}) = \sigma_{y0}\left[1 - \left(\frac{kT}{\Delta E_{b0}} ln\frac{\dot{\varepsilon}_0}{\dot{\varepsilon}}\right)^{2/3}\right] \tag{7}$$

$$\sigma_{y0} = 0.051\alpha^{-1/3}\mu(T)\left(\frac{1+\nu}{1-\nu}\right)^{4/3}\left(\sum_i \frac{c_i \Delta V_i^2}{b^6}\right)^{2/3} \tag{8}$$

$$\Delta E_{b0} = 0.274\alpha^{1/3}\mu(T)\left(\frac{1+\nu}{1-\nu}\right)^{2/3}\left(\sum_i \frac{c_i \Delta V_i^2}{b^6}\right)^{1/3} \quad (9)$$

where $\alpha = 1/8$ is a coefficient related to the dislocation line tension $\Gamma = \alpha\mu b^2$, $\mu(T)$ is the alloy shear modulus at temperature T, $\upsilon = \upsilon(T)$ is the Poisson ratio, and all the numerical factors are entirely derived. The shear modulus μ and Poisson ratio υ of the as-fabricated FeCoNi MEA at room temperature is 60 GPa and 0.35, respectively reported by Wu et al. [17]. The Burgers vector b for the FeCoNi MEA at room temperature is 2.524 [65] and these materials constants is independent of the grain structure of the MEA. It can be seen from equations (7)–(9), the solution strength can only affect by its inherent materials properties. This gives an explanation that the SRS exponent of the MEA at nanoscale is not changed. And the SRS exponent can be written as $m = \frac{d(ln\sigma_y)}{d(ln\dot{\varepsilon})} = \frac{ln\sigma_y - ln\sigma_{y0}}{ln\dot{\varepsilon} - ln\dot{\varepsilon}_0}$, where the σ_{y0} is the yield strength of the MEA deformed with the strain rate of $\dot{\varepsilon}_0$. The yield strength of the MEA with fixed grain size deformed at known strain rate $\dot{\varepsilon}$ can be calculated and predicted by $\sigma_y = e^{\left(mln\frac{\dot{\varepsilon}}{\dot{\varepsilon}_0} + ln\sigma_{y0}\right)}$. In-depth analysis of the deformation mechanisms of the MEA at nanoscale can be conducted in the future for modelling the plastic deformation of the heterogeneous gradient nanograined MEA at multiple length scales.

5. Conclusions

In this study, we propose a two-level gradient heterogenous nanograined structure for overcoming strength-ductility trade-off of the medium entropy alloy at multiple length scales and demonstrate a novel method to realize it by using the ultrasonic assisted cyclic thermal dynamic solid-state physical process at ambient temperature. We conduct the systematic investigations on the mechanical behaviors of the gradient heterogenous nanocrystalline MEA alloy at multiple length scales from nano to the micro scale via nanoindentation and micropillar compression test. Major conclusions are as follows:

(a) Gradient heterogenous bulk nanocrystalline FeCoNi MEA can be efficiently fabricated by using the proposed ultrasonic assisted cyclic thermal dynamic solid-state physical process; The yield strength of the as-fabricated heterogenous NC MEA can reach as high as 1.48 GPa, which is ~8 times higher than that of the coarse-grained matrix materials and the ultimate strength of the as-fabricated heterogeneous nanograined MEA is 1.7 GPa with a ductility of 45% in compression;
(b) The gradient NC structure of the as-fabricated FeCoNi MEA has been characterized by using the transmission electron microscope. And the elastically homogenous however plastically gradient characteristics of this gradient heterogenous NC MEA alloy has been identified and quantified by using the nanomechanical testing system; This gradient mechanical property can increase the mechanical strength of the entire component while maintenance reasonable ductility at macroscale;
(c) High density grain boundaries are attributed to the strengthen mechanism of the heterogenous NC MEA and it obeys Hall-Patch relationship at nanoscale. We formulate the Hall-Patch equation describing the mathematic relationship between the yield strength and grain size of the FeCoNi MEA at nanoscale successfully;
(d) There is no significant change of the SRS exponent for the MEA with different grain structure and the SRS exponent for the FeCoNi MEA with the average grain structure from 60 nm to several micrometers is ~0.02, which implies that dislocation-mediated deformation mechanism stills dominants at nanoscale for the MEA

Declaration of competing interest

The authors declare that they have no known competing financial interests or personal relationships that could have appeared to influence the work reported in this paper.

Acknowledgements

The authors would like to thank the supports from the Hubei Key Laboratory of Automotive Parts at Wuhan University of Technology, School of Mechanical Engineering and School of Industrial Engineering at Purdue University.

Appendix A. Supplementary data

Supplementary data to this article can be found online at https://doi.org/10.1016/j.msea.2021.141631.

Funding

This research did not receive any specific grant from funding agencies in the public, commercial, or not-for-profit sectors.

Credit author statement

F.Y. and G.J.C. developed the conceptual idea. F.Y., H.L., F.X, and S. H. carried out experiments and characterization. S.X. performed MD simulation under guidance of G.J.C. F.Y. and GJC wrote the manuscript together. The project was overseen by H.L. and G.J.C.

References

[1] Y.F. Ye, Q. Wang, J. Lu, C.T. Liu, Y. Yang, High-entropy alloy: challenges and prospects, Mater. Today 19 (6) (2016) 349–362.
[2] J. Yeh, S. Chen, S. Lin, J. Gan, T. Chin, T. Shun, C. Tsau, S. Chang, Nanostructured high-entropy alloys with multiple principal elements: novel alloy design concepts and outcomes, Adv. Eng. Mater. 6 (5) (2004) 299–303.
[3] E.P. George, D. Raabe, R.O. Ritchie, High-entropy alloys, Nature Reviews Materials 4 (8) (2019) 515–534.
[4] N.D. Stepanov, N.Y. Yurchenko, V. Sokolovsky, M.A. Tikhonovsky, G.A. Salishchev, An AlNbTiVZr0.5 high-entropy alloy combining high specific strength and good ductility, Mater. Lett. 161 (2015) 136–139.
[5] B. Gludovatz, A. Hohenwarter, D. Catoor, E.H. Chang, E.P. George, R.O. Ritchie, A fracture-resistant high-entropy alloy for cryogenic applications, Science 345 (6201) (2014) 1153–1158.
[6] K.R. Lim, K.S. Lee, J.S. Lee, J.Y. Kim, H.J. Chang, Y.S. Na, Dual-phase high-entropy alloys for high-temperature structural applications, J. Alloys Compd. 728 (2017) 1235–1238.
[7] L. Sun, R.J. Cava, High Entropy Alloy Superconductors – Status, Opportunities and Challenges, 2019 arXiv: Superconductivity.
[8] S. Marik, K. Motla, M. Varghese, K.P. Sajilesh, D. Singh, Y. Breard, P. Boullay, R. P. Singh, Superconductivity in a New Hexagonal High Entropy Alloy, 2019 arXiv: Superconductivity.
[9] O. Elatwani, N. Li, M. Li, A. Devaraj, J.K. Baldwin, M.M. Schneider, D. Sobieraj, J. S. Wrobel, D. Nguyenmanh, S.A. Maloy, Outstanding radiation resistance of tungsten-based high-entropy alloys, Science Advances 5 (3) (2019).
[10] G. Laplanche, P. Gadaud, C. Barsch, K. Demtroder, C. Reinhart, J. Schreuer, E. P. George, Elastic moduli and thermal expansion coefficients of medium-entropy subsystems of the CrMnFeCoNi high-entropy alloy, J. Alloys Compd. 746 (2018) 244–255.
[11] J. Peng, Z. Li, L. Fu, X. Ji, Z. Pang, A. Shan, Carbide precipitation strengthening in fine-grained carbon-doped FeCoCrNiMn high entropy alloy, J. Alloys Compd. 803 (2019) 491–498.
[12] E.J. Pickering, R. Munozmoreno, H.J. Stone, N.G. Jones, Precipitation in the equiatomic high-entropy alloy CrMnFeCoNi, Scripta Mater. 113 (2016) 106–109.
[13] Y. Kim, J. Choe, K. Lee, Selective laser melted equiatomic CoCrFeMnNi high-entropy alloy: microstructure, anisotropic mechanical response, and multiple strengthening mechanism, J. Alloys Compd. 805 (2019) 680–691.
[14] M.A. Melia, J. Carroll, S.R. Whetten, S.N. Esmaeely, J. Locke, E.M.H. White, I. E. Anderson, M. Chandross, J.R. Michael, N. Argibay, Mechanical and corrosion properties of additively manufactured CoCrFeMnNi high entropy alloy, Additive manufacturing 29 (2019) 100833.
[15] H. Luo, S.S. Sohn, W. Lu, L. Li, X. Li, C.K. Soundararajan, W. Krieger, Z. Li, D. Raabe, A strong and ductile medium-entropy alloy resists hydrogen embrittlement and corrosion, Nat. Commun. 11 (1) (2020) 3081.

[16] W. Li, T.-H. Chou, T. Yang, W.-S. Chuang, J.C. Huang, J. Luan, X. Zhang, X. Huo, H. Kong, Q. He, X. Du, C.-T. Liu, F.-R. Chen, Design of ultrastrong but ductile medium-entropy alloy with controlled precipitations and heterogeneous grain structures, Applied Materials Today 23 (2021) 101037.
[17] Z. Wu, H. Bei, G.M. Pharr, E.P. George, Temperature dependence of the mechanical properties of equiatomic solid solution alloys with face-centered cubic crystal structures, Acta Mater. 81 (2014) 428–441.
[18] Z. Fu, L. Jiang, J.L. Wardini, B.E. MacDonald, H. Wen, W. Xiong, D. Zhang, Y. Zhou, T.J. Rupert, W. Chen, A high-entropy alloy with hierarchical nanoprecipitates and ultrahigh strength, Sci. Adv. 4 (10) (2018) eaat8712.
[19] T. Yang, Y. Zhao, Y. Tong, Z. Jiao, J. Wei, J. Cai, X. Han, D. Chen, A. Hu, J. Kai, Multicomponent intermetallic nanoparticles and superb mechanical behaviors of complex alloys, Science 362 (6417) (2018) 933–937.
[20] Z. Li, K.G. Pradeep, Y. Deng, D. Raabe, C.C. Tasan, Metastable high-entropy dual-phase alloys overcome the strength–ductility trade-off, Nature 534 (7606) (2016) 227–230.
[21] H. Gleiter, Nanocrystalline Materials, Advanced Structural and Functional Materials, Springer1991, pp. 1-37.
[22] M.A. Meyers, A. Mishra, D.J. Benson, Mechanical properties of nanocrystalline materials, Prog. Mater. Sci. 51 (4) (2006) 427–556.
[23] K. Lu, Stabilizing nanostructures in metals using grain and twin boundary architectures, Nat. Rev. Mater. 1 (5) (2016) 1–13.
[24] M.J.R. Haché, C. Cheng, Y. Zou, Nanostructured high-entropy materials, J. Mater. Res. 35 (8) (2020) 1051–1075.
[25] X. Zhou, X. Li, K. Lu, Enhanced thermal stability of nanograined metals below a critical grain size, Science 360 (6388) (2018) 526–530.
[26] A.R. Kalidindi, C.A. Schuh, Stability criteria for nanocrystalline alloys, Acta Mater. 132 (2017) 128–137.
[27] Y. Wei, Y. Li, L. Zhu, Y. Liu, X. Lei, G. Wang, Y. Wu, Z. Mi, J. Liu, H. Wang, Evading the strength–ductility trade-off dilemma in steel through gradient hierarchical nanotwins, Nat. Commun. 5 (1) (2014) 1–8.
[28] T. Fang, W. Li, N. Tao, K. Lu, Revealing extraordinary intrinsic tensile plasticity in gradient nano-grained copper, Science 331 (6024) (2011) 1587–1590.
[29] H. Huang, Z. Wang, J. Lu, K. Lu, Fatigue behaviors of AISI 316L stainless steel with a gradient nanostructured surface layer, Acta Mater. 87 (2015) 150–160.
[30] Y.B. Lei, Z. Wang, J. Xu, K. Lu, Simultaneous enhancement of stress- and strain-controlled fatigue properties in 316L stainless steel with gradient nanostructure, Acta Mater. 168 (2019) 133–142.
[31] H. Ueno, K. Kakihata, Y. Kaneko, S. Hashimoto, A. Vinogradov, Enhanced fatigue properties of nanostructured austenitic SUS 316L stainless steel, Acta Mater. 59 (18) (2011) 7060–7069.
[32] J. Zhou, Z. Sun, P. Kanoute, D. Retraint, Effect of surface mechanical attrition treatment on low cycle fatigue properties of an austenitic stainless steel, Int. J. Fatig. 103 (2017) 309–317.
[33] P. Cao, The strongest size in gradient nanograined metals, Nano Lett. 20 (2) (2020) 1440–1446.
[34] J. Hu, Y. Shi, X. Sauvage, G. Sha, K. Lu, Grain boundary stability governs hardening and softening in extremely fine nanograined metals, Science 355 (6331) (2017) 1292–1296.
[35] E. Ma, X. Wu, Tailoring heterogeneities in high-entropy alloys to promote strength–ductility synergy, Nat. Commun. 10 (1) (2019) 1–10.
[36] K. Lu, Making strong nanomaterials ductile with gradients, Science 345 (6203) (2014) 1455–1456.
[37] V. Maier, K. Durst, J. Mueller, B. Backes, H.W. Höppel, M. Göken, Nanoindentation strain-rate jump tests for determining the local strain-rate sensitivity in nanocrystalline Ni and ultrafine-grained Al, J. Mater. Res. 26 (11) (2011) 1421–1430.
[38] F. Yin, G.J. Cheng, R. Xu, K. Zhao, Q. Li, J. Jian, S. Hu, S. Sun, L. An, Q. Han, Ultrastrong nanocrystalline stainless steel and its Hall-Petch relationship in the nanoscale, Scripta Mater. 155 (2018) 26–31.
[39] F. Yin, S. Hu, L. Hua, X. Wang, S. Suslov, Q. Han, Surface nanocrystallization and numerical modeling of low carbon steel by means of ultrasonic shot peening, Metall. Mater. Trans. 46 (3) (2015) 1253–1261.
[40] F. Yin, Y. Liu, R. Xu, K. Zhao, A. Partin, Q. Han, Nanograined surface fabricated on the pure copper by ultrasonic shot peening and an energy-density based criterion for peening intensity quantification, J. Manuf. Process. 32 (2018) 656–663.
[41] F. Yin, R. Xu, S. Hu, K. Zhao, S. Yang, S. Kuang, Q. Li, Q. Han, Enhanced mechanical and biological performance of an extremely fine nanograined 316L stainless steel cell–substrate interface fabricated by ultrasonic shot peening, ACS Biomater. Sci. Eng. 4 (5) (2018) 1609–1621.
[42] S. Yoshida, T. Ikeuchi, T. Bhattacharjee, Y. Bai, A. Shibata, N. Tsuji, Effect of elemental combination on friction stress and Hall-Petch relationship in face-centered cubic high/medium entropy alloys, Acta Mater. 171 (2019) 201–215.
[43] P. Sathiyamoorthi, H.S. Kim, High-entropy alloys with heterogeneous microstructure: processing and mechanical properties, Prog. Mater. Sci. (2020) 100709.
[44] B. Schuh, F. Mendez-Martin, B. Völker, E.P. George, H. Clemens, R. Pippan, A. Hohenwarter, Mechanical properties, microstructure and thermal stability of a nanocrystalline CoCrFeMnNi high-entropy alloy after severe plastic deformation, Acta Mater. 96 (2015) 258–268.
[45] S. Sun, Y. Tian, X. An, H. Lin, J. Wang, Z. Zhang, Ultrahigh cryogenic strength and exceptional ductility in ultrafine-grained CoCrFeMnNi high-entropy alloy with fully recrystallized structure, Mater. Today Nano 4 (2018) 46–53.
[46] X. Xu, P. Liu, A. Hirata, S. Song, T. Nieh, M. Chen, Microstructural origins for a strong and ductile Al0. 1CoCrFeNi high-entropy alloy with ultrafine grains, Materialia 4 (2018) 395–405.
[47] M. Yang, D. Yan, F. Yuan, P. Jiang, E. Ma, X. Wu, Dynamically reinforced heterogeneous grain structure prolongs ductility in a medium-entropy alloy with gigapascal yield strength, Proc. Natl. Acad. Sci. Unit. States Am. 115 (28) (2018) 7224–7229.
[48] S. Yoshida, T. Bhattacharjee, Y. Bai, N. Tsuji, Friction stress and Hall-Petch relationship in CoCrNi equi-atomic medium entropy alloy processed by severe plastic deformation and subsequent annealing, Scripta Mater. 134 (2017) 33–36.
[49] W. Lu, X. Luo, Y. Yang, B. Huang, Hall-petch relationship and heterogeneous strength of CrCoNi medium-entropy alloy, Mater. Chem. Phys. (2020) 123073.
[50] J. Li, B. Gao, Y. Wang, X. Chen, Y. Xin, S. Tang, B. Liu, Y. Liu, M. Song, Microstructures and mechanical properties of nano carbides reinforced CoCrFeMnNi high entropy alloys, J. Alloys Compd. 792 (2019) 170–179.
[51] F. Yin, S. Hu, R. Xu, X. Han, D. Qian, W. Wei, L. Hua, K. Zhao, Strain rate sensitivity of the ultrastrong gradient nanocrystalline 316L stainless steel and its rate-dependent modeling at nanoscale, Int. J. Plast. (2020) 102696.
[52] Z. Liang, X. Wang, W. Huang, M. Huang, Strain rate sensitivity and evolution of dislocations and twins in a twinning-induced plasticity steel, Acta Mater. 88 (2015) 170–179.
[53] V. Maier-Kiener, K. Durst, Advanced nanoindentation testing for studying strain-rate sensitivity and activation volume, JOM (J. Occup. Med.) 69 (11) (2017) 2246–2255.
[54] J. Chen, L. Lu, K. Lu, Hardness and strain rate sensitivity of nanocrystalline Cu, Scripta Mater. 54 (11) (2006) 1913–1918.
[55] M. Dao, L. Lu, Y. Shen, S. Suresh, Strength, strain-rate sensitivity and ductility of copper with nanoscale twins, Acta Mater. 54 (20) (2006) 5421–5432.
[56] S. Cheng, E. Ma, Y. Wang, L. Kecskes, K. Youssef, C. Koch, U. Trociewitz, K. Han, Tensile properties of in situ consolidated nanocrystalline Cu, Acta Mater. 53 (5) (2005) 1521–1533.
[57] N. Wang, Z. Wang, K. Aust, U. Erb, Room temperature creep behavior of nanocrystalline nickel produced by an electrodeposition technique, Mater. Sci. Eng., A 237 (2) (1997) 150–158.
[58] H. Tanimoto, S. Sakai, H. Mizubayashi, Mechanical property of high density nanocrystalline gold prepared by gas deposition method, Nanostruct. Mater. 12 (5–8) (1999) 751–756.
[59] D. Jia, K. Ramesh, E. Ma, Effects of nanocrystalline and ultrafine grain sizes on constitutive behavior and shear bands in iron, Acta Mater. 51 (12) (2003) 3495–3509.
[60] T. Malow, C. Koch, P. Miraglia, K. Murty, Compressive mechanical behavior of nanocrystalline Fe investigated with an automated ball indentation technique, Mater. Sci. Eng., A 252 (1) (1998) 36–43.
[61] D. Jang, M. Atzmon, Grain-size dependence of plastic deformation in nanocrystalline Fe, J. Appl. Phys. 93 (11) (2003) 9282–9286.
[62] Q. Wei, T. Jiao, S. Mathaudhu, E. Ma, K. Hartwig, K. Ramesh, Microstructure and mechanical properties of tantalum after equal channel angular extrusion (ECAE), Mater. Sci. Eng., A 358 (1–2) (2003) 266–272.
[63] Q. Wei, T. Jiao, K. Ramesh, E. Ma, Nano-structured vanadium: processing and mechanical properties under quasi-static and dynamic compression, Scripta Mater. 50 (3) (2004) 359–364.
[64] E.P. George, W. Curtin, C.C. Tasan, High entropy alloys: a focused review of mechanical properties and deformation mechanisms, Acta Mater. 188 (2020) 435–474.
[65] C. Varvenne, A. Luque, W.A. Curtin, Theory of strengthening in fcc high entropy alloys, Acta Mater. 118 (2016) 164–176.